Tradeoff of Spectral and Energy Efficiencies: Impact of Power Amplifier on OFDM Systems

Jingon Joung, Chin Keong Ho, and Sumei Sun
Institute for Infocomm Research (I[2]R), A*STAR, Singapore
E-mail: {jgjoung,hock,sunsm}@i2r.a-star.edu.sg

***Abstract*—Spectral efficiency (SE) and energy efficiency (EE) are key measures for wireless communication systems. In OFDM systems, the non-linear effects and inefficiencies of power amplifiers (PAs) have posed practical challenges for system design. In this paper, we analyze the impact of the PA on the SE and EE tradeoff of OFDM systems. We also propose a PA switching technique which achieves a better SE-EE tradeoff, e.g., the EE can be improved by 323% with 15% SE reduction.**

***Index Terms*—Energy efficiency, spectral efficiency, OFDM, power amplifier, power amplifier switching.**

I. Introduction

Wireless access communication networks consume significant amount of energy to overcome fading and interference, compared to fixed line networks [1]. In wireless networks, energy is mostly consumed at the base station (BS) [2], of which 50%–80% of power consumption is consumed at power amplifiers (PAs) [3]. Fig. 1 plots PA output power $P_{\rm out}$ versus PA power consumption $P_{\rm PA}$, based on our survey of commercially available PAs for which we give a summary of the key parameters in Table I in the Appendix. A measure of the PA efficiency is given by the drain efficiency $\eta = P_{\rm out}/P_{\rm PA}$. From Fig. 1, we see that η is typically between 20% and 30%, which confirms that the overhead incurred at PA is substantial. To ensure high energy efficiency (EE), the PA characteristics have to be carefully considered in system designs.

On the other hand, high spectral efficiency (SE) is needed to support the growing demands of high data traffic. To support high SE in wireless fading channels, orthogonal frequency division multiplex (OFDM) and orthogonal frequency division multiple access (OFDMA) systems remain as popular choices. However, OFDM and OFDMA modulated signals exhibit high peak-to-average power ratio (PAPR). To circumvent the resulting performance degradation, input backoff (IBO) is implemented by reducing the input power. In order to retain high SE, this popular technique of IBO in turn results in a reduction of EE, because PAs are operate at high efficiency when it is near its power saturation point [4]–[6]. Hence, a SE-EE tradeoff exists when the optimization is performed with respect to the PA. It is thus important to jointly characterize the role that a PA plays in both SE and EE of wireless communication systems.

In this paper, we quantify the impact of PA on the degradation of both SE and EE in practice. To do this, it is essential to have a sufficiently accurate, yet tractable, model for the PA (i) on its *non-linearity behavior*, and (ii) on its *imperfect efficiency*

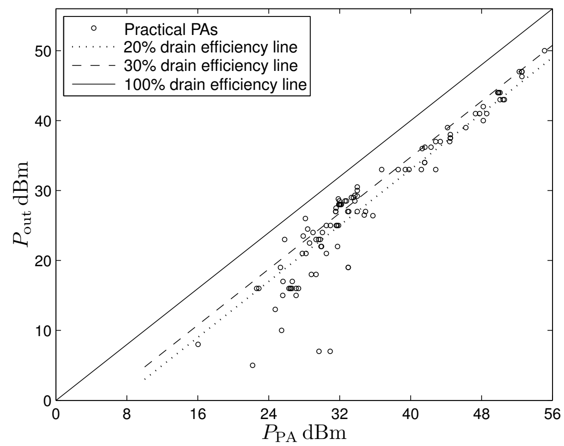

Fig. 1. Maximum output power (at the linear region) versus consumed power $P_{\rm PA}$ for commercially available PAs in Table I in Appendix.

to specify the relationship of $P_{\rm PA}$ and the transmission power $P_{\rm out}$, i.e., $P_{\rm PA} > P_{\rm out}$ and $\eta < 100\%$. To provide tractable results, we assume that the non-linearity of the PA is modeled by a soft limiter [7], i.e., the output is clipped to a constant if the input signal exceeds a threshold value, and experiences a linear scaling of its input otherwise. As a consequence, we obtain a closed-form expression of SE which allows numerical evaluation. We also establish a PA-dependent (class-A, class-B, and Doherty Types) nonlinear power consumption model from various recent studies on empirical power measurement and parameters for cellular and wireless local area networks [8]–[12] and derive the EE. From the analysis and numerical evaluation, we observe that the practical PA can support a narrow SE-EE tradeoff with only a limited range of SE. In cellular communications, however, a wide range of SE-EE tradeoff is desired because the BSs need high data rates intermittently, yet need to save energy whenever possible to save operation costs. To achieve a wide Pareto-optimal SE-EE tradeoff region, we propose a PA switching (selection or time sharing) technique, in which one or more PAs are switched on at any time between frames to maximize the EE while satisfying the required SE. As a result, the degree of freedom offered from the multiple PAs yields a high EE over a wide range of SE. Numerical results show that the SE-EE tradeoff improvement is significant even though practical losses are considered, such as switch insertion loss and switching time overhead.

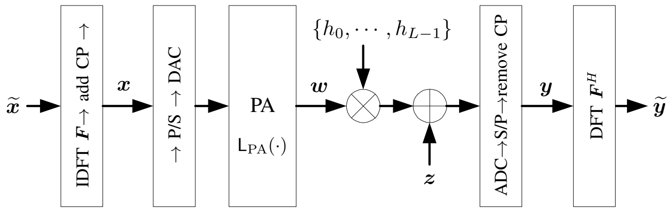

Fig. 2. An OFDM system with a non-linear memoryless power amplifier (PA) represented by function $\mathsf{L}_{\mathrm{PA}}(\cdot)$.

II. Signal Model

Consider the OFDM system with a non-linear memoryless PA shown in Fig. 2. Without loss of generality (w.l.o.g.), we consider the transmission of one OFDM symbol consisting of N complex-valued data symbols $\widetilde{\boldsymbol{x}} = [\widetilde{x}_0, \cdots, \widetilde{x}_{N-1}]^T$, over a total frequency band of Ω Hz. The data symbol $\widetilde{x}_n$ is sent on the nth orthogonal subcarrier. The data symbols are assumed to be identical and independently distributed (i.i.d.) subject to the power constraint $\mathrm{E}[|\widetilde{x}|^2] \leq P_{\mathrm{in}}$; here and subsequently, we drop the subcarrier or time index if there is no dependence or when there is no ambiguity. We transform $\widetilde{\boldsymbol{x}}$ to the time domain signal vector $\boldsymbol{x} = [x_0, \cdots, x_{N-1}]^T$ according to $\boldsymbol{x} = \boldsymbol{F}\widetilde{\boldsymbol{x}}$, where $\boldsymbol{F}$ is the N-by-N unitary inverse discrete Fourier transform (IDFT) matrix. Thus, $\mathrm{E}[|x|^2] \leq P_{\mathrm{in}}$. Then a cyclic prefix (CP) of length N_{CP} is added to $\boldsymbol{x}$ and passed to a parallel-to-serial converter (P/S), followed by a digital-to-analogue converter (DAC). We assume the DAC, analogue-to-digital converter (ADC) and subsequent processing (such as timing and frequency synchronization) are ideal such that we may use x_t to represent the output of the DAC at discrete time index t. We write $x_t = a_t e^{j\theta_t}$ where $a_t \triangleq |x_t|$ is its amplitude and $0 \leq \theta_t < 2\pi$ is its phase.

Next, the DAC output x_t is amplified through a memoryless PA described by the non-linear function $\mathsf{L}_{\mathrm{PA}}(\cdot)$ to give the output $w_t = \mathsf{L}_{\mathrm{PA}}(x_t)$ at time t, denoted collectively by the vector $\boldsymbol{w} = [w_0, \cdots, w_{N+N_{\mathsf{CP}}-1}]^T$. We assume there is no phase distortion, since typically its effect is small compared to the amplitude distortion [4]. To ease analysis, assuming the perfect linearization in low power regime, we can use the *soft limiter model* [7], [13], which is the simplest model that can capture the amplitude distortion (clipping effect) as follows:

$$\mathsf{L}_{\mathrm{PA}}(a_t) = \begin{cases} \sqrt{g}a_t, & \text{if } a_t < a_{\max}, \\ b_{\max}, & \text{if } a_t \geq a_{\max}, \end{cases} \tag{1}$$

where $\sqrt{g} \geq 1$ is a parameter interpreted as the desired linear gain, $a_{\max} \triangleq \sqrt{P_{\mathrm{in}}^{\max}}$, and $b_{\max} \triangleq \sqrt{P_{\mathrm{out}}^{\max}}$. Under this model, we can write $w_t = b_t e^{j\theta_t}$ where $b_t \triangleq |w_t|$ while the phase remains the same as that of x_t.

Finally, the PA output is transmitted through a L-tap multi-path channel $\{h_0, h_1, \cdots, h_{L-1}\}$, where we assume $L \leq N_{\mathsf{CP}}$. Assuming perfect timing synchronization, the CP is removed and the received signal is then

$$y_t = h_t \otimes w_t + z_t \triangleq r_t e^{j\phi} \tag{2}$$

for $t = 0, \cdots, N-1$. Here, $\otimes$ is the circular convolution operator, $z_t \sim \mathcal{CN}(0, \sigma_z^2)$ is an additive white Gaussian noise (AWGN), and r_t and ϕ_t represent the amplitude and phase of y_t. The received signal vector $\boldsymbol{y} = [y_0, \cdots, y_{N-1}]^T$ (for convenience, we shift the time indices to start from zero) is then transformed via a DFT to give $\widetilde{\boldsymbol{y}} = [\widetilde{y}_0, \cdots, \widetilde{y}_{N-1}]^T = \boldsymbol{F}^H\boldsymbol{y}$.

Based on the signal model, we shall obtain tractable results which offer insights on how the PA affects the SE and EE in Sections III and IV, respectively. Then we study how this leads to the analysis of a new transmitter architecture in Section IV-C, which offers a better tradeoff in terms of SE and EE.

III. Spectral Efficiency

In this section, we determine the SE of the system in Fig. 2. We ignore the CP overhead for simplicity. We assume the data symbols are i.i.d. with distribution $\widetilde{X} \sim \mathcal{CN}(0, P_{\mathrm{in}})$. Hence the time-domain signals are also i.i.d. with distribution $X \sim \mathcal{CN}(0, P_{\mathrm{in}})$. The time domain signals have high PAPR and thus they are representative of the scenario when a high-order modulation is used or when N is large.

We fix the following PA-related parameters: the maximum power input $P_{\mathrm{in}}^{\max}$; the power loading factor $\xi \triangleq \frac{P_{\mathrm{in}}}{P_{\mathrm{in}}^{\max}}$, $\xi \geq 0$, which is related to the IBO as $\mathrm{IBO} \triangleq 10\log_{10}(\xi^{-1})\,\mathrm{dB}$; and the gain g in the linearity region. Thus the maximum power output $P_{\mathrm{out}}^{\max} = gP_{\mathrm{in}}^{\max}$ is also fixed; for convenience, let $\gamma \triangleq P_{\mathrm{out}}^{\max}/\sigma_z^2 > 0$ be the maximum power output normalized by the noise variance σ_z^2.

We use upper case letters to represent random variables, such as X, W, and Y; we use lower case letters to represent their realizations, such as x, w, and y. The probability density function (pdf) of random variable X is denoted by $f_X(\cdot)$. We recall that we also write the signals in terms of their amplitudes and phases as $x = ae^{j\theta}$, $w = be^{j\theta}$, and $y = re^{j\phi}$.

Specifically, we define SE, in $\mathrm{b/s/Hz}$, as the amount of bits that are reliably decoded per channel use (i.e., per unit bandwidth and per unit time). We define EE, in $\mathrm{b/J}$, as the total amount of bits that are reliably decoded bits normalized by the energy. Thus, SE and EE are given by [14], [15]

$$\mathsf{SE} = \frac{I(\widetilde{\boldsymbol{X}}; \widetilde{\boldsymbol{Y}})}{N} \tag{3a}$$

$$\mathsf{EE} = \frac{T\Omega\,\mathsf{SE}}{TP_{\mathrm{c}}} = \frac{\Omega\,\mathsf{SE}}{P_{\mathrm{c}}} \tag{3b}$$

where $I(\widetilde{\boldsymbol{X}}; \widetilde{\boldsymbol{Y}})$ is the mutual information in $\mathrm{b/s/Hz}$ given the length-N transmitted and received vectors $\widetilde{\boldsymbol{X}}$ and $\widetilde{\boldsymbol{Y}}$, representing an achievable sum rate over N channel uses [16]; T is the total time used; and P_{c} is the total power consumption including P_{PA}.

A. Mutual Information in Flat Fading Channel

Consider a flat fading channel where $L = 1$. Let $h_0 = 1$, w.l.o.g., as the actual channel attenuation and any fixed energy losses incurred can be reflected by changing the noise variance such that the signal-to-noise ratio (SNR) is maintained. Hence the channel model at time index t is

$$Y_t \quad = \quad W_t + Z_t, \quad \text{where } W_t = \mathsf{L}_{\mathrm{PA}}(A_t)e^{\theta_t}. \tag{4}$$

The achievable rate averaged over N transmissions is given by

$$\begin{aligned} I(\widetilde{\boldsymbol{X}};\widetilde{\boldsymbol{Y}})/N &\overset{(a)}{=} I(\boldsymbol{X};\boldsymbol{Y})/N \overset{(b)}{=} \sum_{t=1}^{N} I(X_t;Y_t)/N \\ &\overset{(c)}{=} I(X;Y) \overset{(d)}{=} H(Y) - \log_2 \pi e \sigma_z^2. \end{aligned} \tag{5}$$

Here, (a) follows since the time-domain and frequency-domain signals are related by a unitary transform, (b) follows from the independence of the signals in the time domain (due to the memoryless PA and the i.i.d. transmitted signals and noise), (c) follows since the mutual information is identical over time and so we can drop the time index, and (d) follows from $I(X;Y) = H(Y) - H(Y|X)$ and the conditional entropy $H(Y|X) = H(N) = \log_2 \pi e \sigma_z^2$. Denote S as a binary random variable that denotes if clipping at the PA occurs, i.e., $S = 1$ if $A \geq a_{\max}$ and $S = 0$ otherwise. Since $X = Ae^{j\theta} \sim \mathcal{CN}(0, P_{\mathrm{in}})$, the random variable A follows the Rayleigh distribution. Thus, the probability of S is

$$\begin{aligned} \Pr(S=0) &= \Pr\left(A \leq a_{\max}\right) = 1 - \exp\left(-\xi^{-1}\right) \\ \Pr(S=1) &= 1 - \Pr(S=0) = \exp\left(-\xi^{-1}\right) \end{aligned} \tag{6}$$

The differential entropy of Y is given by [16]

$$H(Y) = -\int_y f_Y(y) \log_2 f_Y(y) dy, \tag{7}$$

where the pdf of y can be written as $f_Y(y) = \sum_{i=0,1} f_Y(y, S=i)$. The numerical computation of the entropy (7) is straightforward given a closed-form expression of $f_Y(y, S=0)$ and $f_Y(y, S=1)$, which are obtained as follows (refer to [17] for the proofs):

$$\begin{aligned} f_Y(y, S{=}0) &= \mathsf{N}_0(y)(1 - \mathsf{Q}_1\left(\sqrt{\mu}, \sqrt{\rho_{\max}}\right)) \\ f_Y(y, S{=}1) &= \mathsf{N}_1(y)\left(\Pr(S=1)\exp\left(\frac{-2b_{\max}y_{\mathrm{Re}}}{\sigma_z^2}\right)\mathsf{I}_0\left(\frac{2b_{\max}|y|}{\sigma_z^2}\right)\right) \end{aligned} \tag{8}$$

where $\mathsf{N}_0(y)$ denotes the pdf of $\mathcal{CN}\left(0, gP_{\mathrm{in}} + \sigma_z^2\right)$; $\mathsf{Q}_1(\cdot,\cdot)$ is the Marcum-Q-function [18] with parameters $\rho_{\max} = \frac{2(gP_{\mathrm{in}}+\sigma_z^2)}{gP_{\mathrm{in}}}\sqrt{b_{\max}}$ and $\mu = \frac{8gP_{\mathrm{in}}(gP_{\mathrm{in}}+\sigma_z^2)}{\sigma_z^4}|y|^2$; $\mathsf{N}_1(y)$ is the pdf of $\mathcal{CN}\left(b_{\max}, \sigma_z^2\right)$; y_{Re} is the real part of y; and $\mathsf{I}_0(\cdot)$ is the modified Bessel function of the first kind [18].

B. Mutual Information in Multipath Channel

We now consider the general case of a L-tap multipath channel, where $L \leq N_{\mathsf{CP}}$. The received signal in the time domain is given by (2). Because the PA non-linearity resulted in a correlated interference in the frequency domain which does not appear to evaluate as a closed-form expression, exact analysis of the mutual information in multipath case is intractable. Instead, we obtain a lower bound for the mutual information, denoted by I_t^{LB}, which is given by the mutual information of the following channel (proof is shown in [17])

$$Y_t' \quad = \quad h_t' \, \mathsf{L}_{\mathrm{PA}}(A_t)e^{\theta_t} + Z_t' \tag{9}$$

where $h_t' = \sqrt{|h_0|^2 + \sum_{i=1}^{L-1} \frac{|h_i|^2}{\sigma_n^2 + gP_{\mathrm{in}}\sum_{j=0}^{i-1}|h_i|^2}}$ is the equivalent channel and $Z_t' \sim \mathcal{CN}(0, \sigma_z^2)$. The channel (9) is simply the flat fading channel (4) with the noise variance modified accordingly. Hence we can obtain I_t^{LB} from (5) directly. Although the lower bound always holds, we can intuitively treat (9) as the channel where the power of all the multipaths are collected and any interference is treated as Gaussian distribution. For the details, refer to [17].

C. Analytical Results on SE

Using (8) into (7), we find $H(Y)$ and get $I(X;Y)$ from (5) in flat fading channel. Similarly, from (9), we can obtain the mutual information of the signal in multipath channel. Using the lower bound of the mutual information, eventually, we can derive the spectral efficiency from (3a). Generally, the SE in (3a) can be represented by the function of ξ as

$$\mathsf{SE}(\xi) = H(Y) - \log_2 \pi e \sigma_z^2 \tag{10}$$

since the conditional probabilities in (8) are functions of $P_{\mathrm{in}} = \xi P_{\mathrm{in}}^{\max}$ and $b_{\max} = \sqrt{gP_{\mathrm{in}}\xi^{-1}}$, i.e., $H(Y)$ is a function of ξ.

By setting $b_{\max} = \sqrt{P_{\mathrm{out}}^{\max}} \to \infty$, we can recover perfectly linear PA as

$$\mathsf{SE}^{\mathrm{ideal}}(\xi) = \log_2\left(1 + \gamma\xi\right) \tag{11}$$

which is the well-known log-shape function.

An approximation of the SE can be obtained if $P_{\mathrm{in}} \ll P_{\mathrm{in}}^{\max}$ or $\xi \ll 1$, which gives $f_Y(y, S=i) \approx \mathsf{N}_i(y)$, $i = 1, 2$, in (8). We note that typically this holds due to the IBO. We call the resulting SE as $\mathsf{SE}^{\mathrm{IBO}}$. We can also show that $\mathsf{SE}^{\mathrm{IBO}}$ is a concave function over $0 < \xi \leq \frac{1}{2}$. From this fact, we can derive the following theorem (refer to [17] for the proofs):

Theorem 1. *The optimal power loading (or equivalently optimal IBO) factor $\xi_{\mathrm{SE}}^{\star}$ which maximizes $\mathsf{SE}^{\mathrm{IBO}}$ is*

$$\xi_{\mathrm{SE}}^{\star} \approx -\mathsf{W}^{-1}\left(\ln^{-1}\left(\pi e \sigma_z^2\right)\right) \tag{12}$$

where $\mathsf{W}(\cdot) \leq -1$ is a Lambert W function [19].

Interestingly, the approximated $\xi_{\mathrm{SE}}^{\star}$ depends only on σ_z^2 as we assume $\xi \ll 1$ in derivation. This makes $\xi_{\mathsf{SE}}^{\star}$ independent of other PA parameters. The typical value of IBO is around $8\,\mathrm{dB}$ in practice, which includes an additional margin for fading channels [10]. Numerical results verify that $\xi_{\mathrm{SE}}^{\star}$ maximizes the true $\mathsf{SE}(\xi)$ effectively as well regardless of the IBO.

IV. Energy Efficiency

To derive the EE of the system in Fig. 2, we use a power consumption model in the literature [8], [9]:

$$P_{\mathrm{c}} = (1 + C_{\mathrm{PS}})(1 + C_{\mathrm{CB}})(P_{\mathrm{BB}} + P_{\mathrm{RF}} + P_{\mathrm{PA}}) \tag{13}$$

where C_{PS} is a power supply coefficient (typically $0.1 \leq C_{\mathrm{PS}} \leq 0.15$) and C_{CB} is an active cooler and battery coefficient (typically less than 0.4); P_{BB}, P_{RF}, and P_{PA} are the measurements of power consumption at a base band module, a radio frequency module, a PA module, respectively. The advantage of this model in (13) is that the power consumption of the PA is separated from the power consumption of other components; therefore, we can modify (13) according to the PA types and the power loading factor. Here, though $P_{\rm PA}$ actually depends on many factors including the specific hardware implementation, direct current (DC) bias condition, load characteristics, operating frequency and PA output power, it is dominated by DC power fed to the PA. Hence, using the drain efficiency η depending on the DC power and PA types [5], [6], we can express $P_{\rm PA}$ as a function of ξ as $P_{\rm PA} = \frac{1}{\eta} g\xi P_{\rm in}^{\max}$. Substituting the $P_{\rm PA}$ to (13), we get a *PA-dependant nonlinear* power consumption model as

$$P_{\rm c}(\xi) = P_{\rm fix} + P_{\rm out}^{\max}\left(c_1 + c_2\sqrt{\xi}\right),\ 0 < \xi \le 1, \qquad (14)$$

where $P_{\rm fix} = (1 + C_{\rm PS})(1 + C_{\rm CB})(P_{\rm BB} + P_{\rm RF})$, and the parameters (c_1, c_2) are: $\left(\frac{\pi}{2}c, 0\right)$ for class A; $(0, c)$ for class B; $\left(0, \frac{c}{\ell}\right)$ if $0 < \xi \le \frac{1}{\ell^2}$ or $\left(-\frac{c}{\ell}, \frac{(\ell+1)c}{\ell}\right)$ if $\frac{1}{\ell^2} < \xi \le 1$ for ℓ-way Doherty type. Here, $P_{\rm fix}$ and c can be obtained from empirical results in [10]–[12].

A. Energy Efficiency

Using the SE in (10) and the total power consumption $P_{\rm c}(\xi)$ in (14), we can rewrite the EE in (3b) as a function of ξ as

$$\mathsf{EE}(\xi) = \frac{\Omega \mathsf{SE}(\xi)}{P_{\rm c}(\xi)}. \qquad (15)$$

For comparison and further analysis, the upper bound of $\mathsf{EE}(\xi)$ is given for a perfectly linear PA as

$$\mathsf{EE}(\xi) \le \mathsf{EE}^{\rm linear}(\xi) \triangleq \frac{\Omega \mathsf{SE}^{\rm ideal}(\xi)}{P_{\rm c}(\xi)}. \qquad (16)$$

B. Analytical Results on EE

From the fact that $\mathsf{EE}^{\rm linear}(\xi)$ is a piecewise quasi-concave function over ξ, we can derive the following theorem (proofs are in [17]).

Theorem 2. *The optimal $\xi_{\rm EE}^\star$ maximizing $\mathsf{EE}^{\rm linear}(\xi)$ is as follows: for class A $\xi_{\rm EE}^\star = 1$; for class B $\xi_{\rm EE}^\star = \frac{1}{\gamma}\exp\left(2 + 2\mathsf{W}_0\left(\frac{\sqrt{\gamma}P_{\rm fix}}{eP_{\rm out}^{\max}c}\right)\right)$; for ℓ-way Doherty $\xi_{\rm EE}^\star = \frac{1}{\gamma}\exp\left(2 + 2\mathsf{W}_0\left(\frac{\ell\sqrt{\gamma}(P_{\rm fix}+P_{\rm out}^{\max}c_1)}{eP_{\rm out}^{\max}c_2}\right)\right)$ if $\frac{\partial \mathsf{EE}^{linear}(\xi)}{\partial \xi} = 0$ at $\xi \ne 1$, or $\xi_{\rm EE}^\star = \arg\max_{\xi\in\{\ell^{-2},1\}}\left(\mathsf{EE}^{linear}(\xi)\right)$ if $\frac{\partial \mathsf{EE}^{linear}(\xi)}{\partial \xi} = 0$ at $\xi = 1$, or $\xi_{\rm EE}^\star = \frac{1}{\ell^2}$ if $\frac{\partial \mathsf{EE}^{linear}(\xi)}{\partial \xi} \ne 0$. Here $\mathsf{W}_0(\cdot) \ge -1$ is a Lambert W function.*

Numerical results verify that $\xi_{\rm EE}^\star$ maximizes the true $\mathsf{EE}(\xi)$ effectively as well.

C. SE-EE Tradeoff and PA Switching Methods

In contrast to the ideal SE-EE tradeoff in (3) which is a decreasing convex function, the practical SE-EE in (15) has a concave shape as shown in Fig. 5 later. We observe that typically the EE drops rapidly when the SE exceeds beyond some threshold (which corresponds to the SE when the power of the PA approaches saturation). Thus, the PA can support a narrow SE-EE tradeoff with only a limited range of SE. In cellular communications, a wide range of SE-EE tradeoff is required because the BSs need high data rates intermittently or low data rates with low energy consumption. This motivates the use of multiple PAs, where any PA is switched on at any time between frames by using a switch. We call this technique *PA switching*. The switch insertion loss G_S causes EE and SE degradation, and the switching time consumption ϵ causes further degradation. Numerical results in Section V supports the use of PA switching to achieve significant improvement of the SE-EE tradeoff even after considering the losses incurred in the switching.

V. Numerical Evaluation and Discussion

Numerical results for SE-EE tradeoff are obtained by varying the powr loading factor ξ. We also evaluate the PA switching method based on the two PAs in Table I: a low power PA SM2122-44L (denoted by $\mathsf{PA}^{\mathsf{low}}$) with $P_{\rm out}^{\max} = 25\,{\rm W}$ and a high power PA SM1720-50 (denoted by $\mathsf{PA}^{\mathsf{high}}$) with $P_{\rm out}^{\max} = 100\,{\rm W}$. Both PAs operate in the $2\,{\rm GHz}$ band and can be used for LTE BSs. Bandwidth is set to $10\,{\rm MHz}$. The channel attenuation is modeled as follows [20]: $G + G_S - 128 + 10\log_{10}(d^{-\alpha})\,{\rm dB}$ where G includes the transceiver feeder loss and antenna gains; and $d^{-\alpha}$ is the path loss where d is the distance in kilometers between a transmitter and a receiver and α is a path loss exponent. In simulations, we set $G = 5\,{\rm dB}$, $\alpha = 3.76$, $d = 200\,{\rm m}$, and $\sigma_z^2 = -174\,{\rm dBm/Hz}$. For the power consumption model, we set $c = 4.7$ and $P_{\rm fix} = 130\,{\rm W}$ [10] to model the marco cell communication systems.

Fig. 3 shows the numerical evaluation of SE. As expected, $\mathsf{SE}^{\rm ideal}(\xi)$ in (11) is an increasing concave (log-shape) function, while $\mathsf{SE}(\xi)$ in (10), the SE modeled by a soft limiter at the PA, is a concave function when $\xi \le \frac{1}{2}$. The SE $\mathsf{SE}^{\rm IBO}$ is illustrated as a dashed line. The optimal $\xi_{\rm SE}^\star$ in (12) yields the highest SE as marked by '$\circ$' (*Theorem 1*), which closely approaches to the true SE $\mathsf{SE}(\xi)$.

Fig. 4 shows EE for various types of PAs: Class-A, class-B, and 2-way Doherty PAs. The dotted lines represent $\mathsf{EE}^{\rm linear}(\xi)$. EE obtained with $\xi_{\rm EE}^\star$ in *Theorem 2* is illustrated by '$\times$' and '$\square$' for $\mathsf{EE}(\xi)$ and $\mathsf{EE}^{\rm linear}(\xi)$, respectively. The results show that $\xi_{\rm EE}^\star$ yields the maximum EE and that $\mathsf{EE}^{\rm linear}(\xi_{\rm EE}^\star) = \mathsf{EE}(\xi_{\rm EE}^\star)$ (which are overlapped in the figure), except class-A PA. This is because the practical EE is maximized in the linear region. From the results, we can surmise that the optimal $\xi_{\rm EE}^\star$ derived under the ideal PA assumption is applicable to maximize the practical EE.

Fig. 5 shows the SE-EE tradeoff with and without PA switching. We assume that PA can be switched once every 20 frames. Each frame length is set to be $10\,{\rm ms}$. The losses incurred in the switching are set as $G_S = 1\,{\rm dB}$ and $\epsilon = 1\,{\rm ms}$. For comparison, ideal switching with $G_S = 0\,{\rm dB}$ and $\epsilon = 0$ is evaluated. The EE can be improved by around 210% (323%) if we reduce SE by 12% (15%) from A to B (C), respectively. In contrast, if a single PA $\mathsf{PA}^{\mathsf{high}}$ is used instead, the EE is improved by around 41% with a 12% reduction of SE from A to D. For simplicity, we assume the fraction of time when any PA is switched on is a continuous value from 0 to 1.

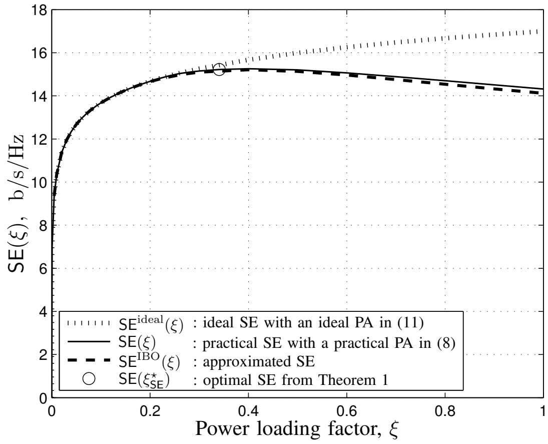

Fig. 3. SE evaluation when PA is high power Doherty with $P_{\text{out}}^{\max} = 25\,\text{W}$ and $g = 55\,\text{dB}$.

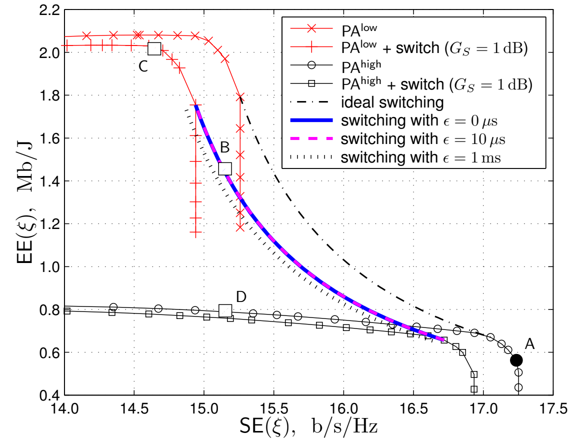

Fig. 5. SE-EE tradeoff with switching PA$^{\text{low}}$ and PA$^{\text{high}}$ when frame length is $10\,\text{ms}$ and 20 frames are transmitted.

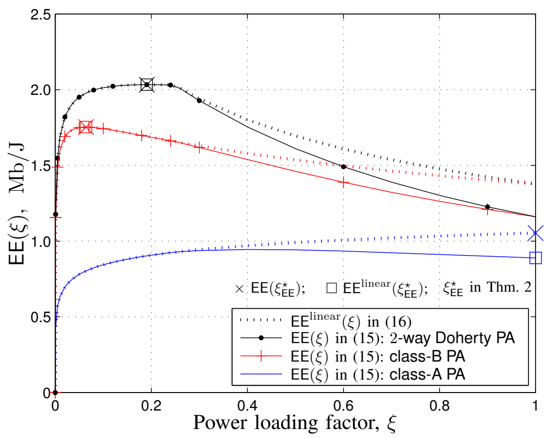

Fig. 4. EE evaluation with $P_{\text{fix}} = 130\,\text{W}$ and $c = 4.7$.

VI. Conclusion

We have given a theoretical analysis of the spectral and energy efficiency (SE-EE) tradeoff, by taking into account the practical non-ideal effects of the power amplifier (PA). This analysis motivates PA switching to achieve a better SE-EE tradeoff, which is verified by numerical results.

References

[1] J. Baliga, R. Ayre, K. Hinton, and R. S. Tucker, "Energy consumption in wired and wireless access networks," *IEEE Commun. Mag.*, vol. 49, pp. 70–77, Jun. 2011.

[2] W. Vereecken, W. V. Heddeghem, M. Deruyck, B. Puype, B. Lannoo, W. Joseph, D. Colle, L. Martens, and P. Demeester, "Power consumption in telecommunication networks: Overview and reduction strategies," *IEEE Commun. Mag.*, vol. 49, pp. 62–69, Jun. 2011.

[3] H. Bogucka and A. Conti, "Degree of freedom for energy savings in practical adaptive wireless systems," *IEEE Commun. Mag.*, vol. 49, pp. 38–45, Jun. 2011.

[4] C. Rapp, "Effects of HPA-nonlinearity on a 4-DPSWOFDM signal for a digital sound broadcasting system," in *Proc. Second European Conference on Satellite Communications*, Lihge, Belgium, Oct. 1991, pp. 179–184.

[5] F. H. Raab, P. Asbeck, S. Cripps, P. B. Kenington, Z. B. Popović, N. Pothecary, J. F. Sevic, and N. O. Sokal, "Power amplifiers and transmitters for RF and microwave," *IEEE Trans. Microwave Theory and Techniques*, vol. 50, pp. 814–826, Mar. 2002.

[6] Y. Yang, J. Cha, B. Shin, and B. Kim, "A fully matched N-Way Doherty amplifier with optimized linearity," *IEEE Trans. Microwave Theory And Techniques*, vol. 51, pp. 986–993, Mar. 2003.

[7] J. Tellado, L. M. C. Hoo, and J. M. Cioffi, "Maximum-likelihood detection of nonlinearly distorted multicarrier symbols by iterative decoding," *IEEE Trans. Communications*, vol. 51, pp. 218–228, Feb. 2003.

[8] O. Arnold, F. Richter, G. Fettweis, and O. Blume, "Power consumption modeling of different base station types in heterogeneous cellular networks," in *Proc. IEEE Future Network and Mobile Summit 2010*, Florence, Italy, Jun, 2010, pp.1–8.

[9] R. V. Raja Kumar and J. Gurugubelli, "How green the LTE technology can be?" in *Proc. IEEE Wireless Communication, Vehicular Technology, Information Theory and Aerospace & Electronic Systems Technology (Wireless VITAE)*, Chennai, India, Feb.–Mar., 2011, pp. 1–5.

[10] G. Auer, V. Giannini, C. Desset, I. Godor, P. Skillermark, M. Olsson, M. A. Imran, D. Sabella, M. J. Gonzalez, O. Blume, and A. Fehske, "How much energy is needed to run a wireless network?" *IEEE Wireless Communications*, vol. 18, pp. 40–49, Oct. 2011.

[11] M. Deruyck, W. Vereecken, E. Tanghe, W. Joseph, M. Pickavet, L. Martens, and P. Demeester, "Comparison of power consumption of mobile WiMAX, HSPA and LTE access networks," in *Proc. IEEE Telecommunications Internet and Media Techno Economics (CTTE)*, Gent, Belgium, Jun. 2010 , pp. 1–7.

[12] F. Richter, A. J. Fehske, and G. P. Fettweis, "Energy efficiency aspects of base station deployment strategies for cellular networks," in *Proc. IEEE Vehicular Technology Conference (VTC-Fall)*, Alaska, USA, Sep. 2009 pp. 1–5.

[13] J. Joung, C. K. Ho, and S. Sun, "Green wireless communications: A power amplifier perspective," in *Proc. Asia Pacific Signal and Information Processing Association (APSIPA) Annual Summit and Conf.*, California, USA, Dec. 2012.

[14] S. Verdú, "Spectral efficiency in the wideband regime," *IEEE Trans. Inf. Theory*, vol. 48. no. 6, pp. 1319–1343, Jun. 2002.

[15] Y. Chen, S. Zhang, S. Xu, and G. Y. Li, "Fundamental trade-offs on green wireless networks," *IEEE Commun. Mag.*, vol. 49, pp. 30–37, Jun. 2011.

[16] T. M. Cover and J. A. Thomas, *Elements of Information Theory*, 2nd ed., New Jersey, John Wiley & Sons, 2006.

[17] J. Joung, C. K. Ho, and S. Sun, "Spectral efficiency and energy efficiency of OFDM systems: Impact of power amplifiers and countermeasures," submitted to *IEEE J. Sel. Areas Commun.*, Apr. 2012.

[18] A. Papoulis and S. Pillai, *Probability, Random Variables and Stochastic Processes*, 4th ed., McGraw-Hill, 2002.

[19] F. Chapeau-Blondeau and A. Monir, "Numerical evaluation of the Lambert W function and application to generation of generalized Gaussian noise with exponent 1/2," *IEEE Trans. Sig. Processing*, vol. 50, pp. 2160–2165, Sep. 2002.

[20] LTE; E-UTRA; RF requirements for LTE Pico Node B (ETSI Tech Rep. 136 931 V9.0.0). [Online] Available: http://www.etsi.org/deliver/

APPENDIX: TABLE I

POWER AMPLIFIER CHARACTERISTICS (ASCENDING ORDER OF $P_{\text{out}}^{\max}$).

PA#	Model	$P_{\text{out}}^{\max}$(dBm)	g(dB)	V_{PA} (Volt)	C_{PA} (mA)	$P_{\text{in}}^{\max}$(dBm)	Frequency (GHz)	Institution
1	MAX2242	5	28.5	3.3	50	10	2.4 – 2.5	MAXIM
2	FMPA2151	7	31	3.3	280	0	2.4 – 2.5	FAIRCHILD Semiconductor
3	FMPA2151	7	33	3.3	375	0	4.9 – 5.9	FAIRCHILD Semiconductor
4	PA1137	8	17	2	20	10	2 – 2.2	tyco Electronics
5	ADL5570	10	29	3.5	100	-	2.3 – 2.4	Analog Devices
6	MAX2242	13	28.5	3.3	90	10	2.4 – 2.5	MAXIM
7	MAX2840	15	22.8	3.3	155	-	5.15 – 5.35	MAXIM
8	BGA6289	15	13	4.1	88	-	1.95 – 2.5	NXP Semiconductors
9	AWT6134	16	23.5	3.4	130	10	1.75 – 1.78	ANADIGICS
10	AWT6138	16	15	3.4	57	10	1.85 – 1.91	ANADIGICS
11	AWT6252	16	24.5	3.4	54	10	1.92 – 1.98	ANADIGICS
12	AWT6252	16	20.5	3.4	54	10	1.92 – 1.98	ANADIGICS
13	RF2192	16	22	3.4	150	10	0.824 – 0.849	EF MICRO-DEVICES
14	RF2196	16	20	3.4	160	10	1.85 – 1.91	EF MICRO-DEVICES
15	RF3163	16	24	3.4	125	10	0.824 – 0.849	EF MICRO-DEVICES
16	RF3164	16	28	3.4	130	10	1.85 – 1.91	EF MICRO-DEVICES
17	RF3165	16	27	3.4	130	10	1.75 – 1.78	EF MICRO-DEVICES
18	RF6100-1	16	26	3.4	135	10	0.824 – 0.849	EF MICRO-DEVICES
19	AP172-317	17	33	3.3	140	20	1.8 – 2.5	SKYWORKS
20	SKY65006	17	30	3.3	110	10	2.4 – 2.5	SKYWORKS
21	RMPA5255	18	33	3.3	230	-	4.9 – 5.9	FAIRCHILD Semiconductor
22	MAX2841	18	22.5	3.3	260	-	5.15 – 5.35	MAXIM
23	FMPA2151	19	31	3.3	600	0	2.4 – 2.5	FAIRCHILD Semiconductor
24	FMPA2151	19	33	3.3	600	0	4.9 – 5.9	FAIRCHILD Semiconductor
25	RMPA2458	19	31.5	3.3	103	5	2.4 – 2.5	FAIRCHILD Semiconductor
26	RF5117	21	26	3	200	10	1.8 – 2.8	EF MICRO-DEVICES
27	RF5189	21	25	3	220	10	2.4 – 2.5	EF MICRO-DEVICES
28	SST13LP01	21	34	3.3	340	-	4.9 – 5.8	Silicon Storage Technology, Inc.
29	RF5117	22	26	3	500	10	1.8 – 2.8	EF MICRO-DEVICES
30	RMPA2455	22	30	5	195	10	2.4 – 2.5	FAIRCHILD Semiconductor
31	MAX2242	22	28.5	3.3	300	10	2.4 – 2.5	MAXIM
32	AP172-317	22.5	33	3.3	220	20	1.8 – 2.5	SKYWORKS
33	MAX2247	23	29.5	3	305	5	2.4 – 2.5	MAXIM
34	SST12LP00	23	27	3.3	115	-	2.4 – 2.5	Silicon Storage Technology, Inc.
35	SST12LP14	23	31	3.3	290	-	2.4 – 2.5	Silicon Storage Technology, Inc.
36	SST13LP01	23	28	3.3	260	-	2.4 – 2.485	Silicon Storage Technology, Inc.
37	AP178-321	23.5	19	3.3	186	20	1.8 – 2.5	SKYWORKS
38	MAX2247	24	29.5	3.3	307	5	2.4 – 2.5	MAXIM
39	AP172-317	24	33	3.3	240	20	1.8 – 2.5	SKYWORKS
40	CX65003	24.5	11.5	5	138	15	1.4 – 2.5	SKYWORKS
41	ADL5570	25	29	3.5	440	-	2.3 – 2.4	Analog Devices
42	ADL5571	25	29	3.3	450	-	2.5 – 2.7	Analog Devices
43	RF2163	25	19	3.3	378	15	1.8 – 2.5	EF MICRO-DEVICES
44	MAX2247	25	30.5	4.2	345	5	2.4 – 2.5	MAXIM
45	SST12LP14	25	31	3.3	340	-	2.4 – 2.5	Silicon Storage Technology, Inc.
46	NE552R479A	26	11	3	217	19	2.45 – 2.45	CEL California Eastern Laboratories
47	PA1153	26.4	28.5	15	250	15	1.8 – 2	tyco Electronics
48	PA1133	26.5	29	15	200	15	1.85 – 1.91	tyco Electronics
49	ADL5571	27	27.5	5	620	-	2.5 – 2.7	Analog Devices
50	RF2114	27	36	6.5	300	12	0.001 – 0.6	EF MICRO-DEVICES
51	RF2161	27	30	3	477	6	1.85 – 2	EF MICRO-DEVICES
52	RF2186	27	31	3	668	6	1.85 – 2	EF MICRO-DEVICES
53	RF5117	27	26	5	500	10	1.8 – 2.8	EF MICRO-DEVICES
54	RF5176	27	26	3	476	6	1.85 – 2	EF MICRO-DEVICES
55	AWT6252	27.5	26.5	3.4	423	10	1.92 – 1.98	ANADIGICS
56	AWT6134	28	26	3.4	475	10	1.75 – 1.78	ANADIGICS
57	AWT6134	28	25	3.4	462	10	1.75 – 1.78	ANADIGICS
58	AWT6138	28	26	3.4	487	10	1.85 – 1.91	ANADIGICS
59	RF3163	28	28.5	3.4	455	10	0.824 – 0.849	EF MICRO-DEVICES
60	RF3164	28	28	3.4	460	10	1.85 – 1.91	EF MICRO-DEVICES
61	RF3165	28	28	3.4	460	10	1.75 – 1.78	EF MICRO-DEVICES
62	RF6100-1	28	29	3.4	465	10	0.824 – 0.849	EF MICRO-DEVICES
63	RF2132	28.5	29	4.8	327	12	0.824 – 0. 849	EF MICRO-DEVICES
64	RF2146	28.5	18.5	4.8	393	12	1.5 – 2	EF MICRO-DEVICES
65	RF6100-4	28.5	28	3.4	535	10	1.85 – 1.91	EF MICRO-DEVICES
66	CX65105	28.5	25	5	470	7	1.7 – 2.2	SKYWORKS
67	SKY65162-70LF	28.8	20	5	306	-	0.869 – 0.96	SKYWORKS
68	RF2192	29	30	3	715	10	0.824 – 0.849	EF MICRO-DEVICES
69	RF2196	29	27	3	755	10	1.85 – 1.91	EF MICRO-DEVICES
70	MGA-43228	29.2	38.5	5	500	-	2.3 – 2.5	Avago Technologies
71	MGA-43328	29.3	37.3	5	470	-	2.5 – 2.7	Avago Technologies
72	AWT6104M5	30	30	3.5	714	10	1.85 – 1.91	ANADIGICS
73	HMC457QS16G/E	30.5	25	5	500	15	2.01 – 2.17	Hittite Microwave corporation
74	HMC453QS16G/E	33	8	6.5	725	-	2.01 – 2.17	Hittite Microwave corporation
75	SM0825-33/33H	33	20	12	1100	4	0.8 – 2.5	Stealth Microwave
76	SM1025-36DMQ2	33	10	12	800	-	1 – 2.5	Stealth Microwave
77	SM1025-37MQ2	33	10	12	1600	-	1 – 2.5	Stealth Microwave
78	PA1110	33	10	10	725	28	1.8 – 2	tyco Electronics
79	PA1132	33	22	12	725	15	1.8 – 2	tyco Electronics
80	SM1727-34HS	34	33	12	1200	1	1.7 – 2.7	Stealth Microwave
81	SM1727-34HSQ	34	36.5	12	1200	1	1.7 – 2.7	Stealth Microwave
82	SM2023-34HS	34	33	12	1200	1	2 – 2.3	Stealth Microwave
83	PA1157	36	24.5	10	1350	15	2 – 2.2	tyco Electronics
84	PA1159	36.2	23.5	10	1700	28	2.3 – 2.4	tyco Electronics
85	PA1162	36.2	30	10	1450	11	0.8 – 0.96	tyco Electronics
86	SM04060-37HS	37	36	12	1800	1	0.4 – 0. 6	Stealth Microwave
87	SM04093-36HS	37	34	12	1600	1	0.4 – 0. 925	Stealth Microwave
88	SM5659-37S	37	20	12	2300	20	5.6 – 5.9	Stealth Microwave
89	SM5759-37HS	37	39	12	2300	2	5.7 – 5.9	Stealth Microwave
90	PA1182	37.5	23	28	1000	15	2.3 – 2.4	tyco Electronics
91	PA1223	37.5	25	28	1000	15	2.11 – 2.17	tyco Electronics
92	PA1224	37.5	25	28	1000	15	2 – 2.2	tyco Electronics
93	PA1186	38	29	28	1000	15	0.8 – 0.96	tyco Electronics
94	XD010-42S-D4F/Y	39	30	28	930	20	0.869 – 0.894	Sirenza Micro Devices
95	SM0822-39	39	45	12	3500	-4	0.8 – 2.2	Stealth Microwave
96	SM0825-40Q	40	39	12	5500	1	0.8 – 2.5	Stealth Microwave
97	SM2023-41	41	55	12	4500	-13	2 – 2.3	Stealth Microwave
98	SM2027-41LS	41	51	12	6000	-7	2 – 2.7	Stealth Microwave
99	SM4450-41L	41	55	12	5000	-13	4.4 – 5	Stealth Microwave
100	SM1822-42LS	42	52	12	5500	-8	1.8 – 2.2	Stealth Microwave
101	SM3338-43	43	50	12	8500	-6	3.3 – 3.8	Stealth Microwave
102	SM5053-43L	43	55	12	9200	-7	5 – 5.3	Stealth Microwave
103	SM7785-43A	43	48	12	9500	-	7.725 – 8.5	Stealth Microwave
104	SM1923-44L	44	55	12	8200	-8	1.9 – 2.3	Stealth Microwave
105	SM2025-44L	44	55	12	8500	-10	2 – 2.5	Stealth Microwave
106	**SM2122-44L**	**44**	**55**	**12**	**8200**	**-9**	**2.1 – 2.2**	**Stealth Microwave**
107	SM2325-44	44	55	12	8000	-10	2.3 – 2.5	Stealth Microwave
108	SM2025-46L	46.3	52	12	15000	-7	2 – 2.5	Stealth Microwave
109	SM04548-47L	47	55	12	14000	-8	0.45 – 0.48	Stealth Microwave
110	SM2023-47L	47	55	12	15000	-7	2 – 2.3	Stealth Microwave
111	SM3134-47L	47	55	12	15000	-6	3.1 – 3.4	Stealth Microwave
112	SM3436-47L	47	56	12	15000	-6	3.4 – 3.6	Stealth Microwave
113	**SM1720-50**	**50**	**50**	**12**	**27000**	**2**	**1.7 – 2**	**Stealth Microwave**